



## OPEN High cycle fatigue limit prediction of machining foreign object damaged TC17 titanium specimen based on the theory of critical distances

Kainan Lu<sup>1</sup>, Yibo Shang<sup>2,3</sup>✉, Chen Wang<sup>2,3</sup>, Bin Li<sup>2,3</sup>, Xiaosheng Zhang<sup>2,3</sup>, Lingfeng Wang<sup>4</sup>, Zhenhua Zhao<sup>5</sup>✉, Liucheng Zhou<sup>3</sup>✉ & Wei Chen<sup>1</sup>

Aircraft engine fans and compressor blades are inevitably subject to external damage during service. It's an important work to predict the high cycle fatigue limit of foreign object damaged blades. In this paper, machining aerofoil specimens were manufactured to simulate the foreign object damaged blade, and the high cycle fatigue limit of machining foreign object damaged TC17 titanium aerofoil specimen were tested at  $3 \times 10^7$  cycles, and a high cycle fatigue limit prediction model of machining foreign object damaged TC17 titanium aerofoil specimen was built based on the theory of critical distances, and compared with the Peterson model. The prediction error is  $9.56 \pm 6.78\%$  for theory of critical distance model and  $59.76 \pm 16.93\%$  for Peterson model. The accuracy of fatigue limit prediction on notched samples using theory of critical distance model is much higher than that of Peterson model, and the theory of critical distances method model is more efficient to evaluate the fatigue strength of notched blade.

**Keywords** Titanium alloy, Foreign object damage, High cycle fatigue limit, The theory of critical distances

When an aircraft engine operates, the high-speed intake airflow often draws foreign hard objects (sand, rivets, and stones et al.) into the engine, resulting in damage to the fan or compressor blades. This type of damage, caused by the impact of hard objects on the engine, is typically called foreign object damage (FOD)<sup>1–5</sup>. FOD can significantly reduce the fatigue limit of blades, leading to unforeseeable fatigue fractures and posing a serious risk to the flight safety<sup>6–8</sup>. Since the 1990s, numerous scholars have researched FOD with experimental simulation methods, numerical simulations and theoretical predictions for damaged blades. Mechanical processing methods are widely used in FOD research due to their simplicity, high repeatability, controllability and cost-effectiveness. Dunham et al.<sup>9</sup> and Nicholas et al.<sup>10</sup> investigated the impact of external material damage notches on fatigue limits during mechanical processing. Studies have revealed that the surface conditions of externally damaged areas created by high-speed impact methods are intricate and exhibit a significant variability in notch shape, size and surface properties. It is difficult to control and predict their influence on fatigue limits.

In contrast, notch machining method is straightforward, controllable and repeatable. Therefore, mechanical machining remains one of the pivotal prefabrication methods for addressing foreign object damage in engineering.

Numerous researchers have investigated the influence of Foreign Object Damage (FOD) on the fatigue limit of blades, providing extensive data for investigation of blade external damage and high-cycle fatigue tests<sup>6,11–13</sup>. It has been discerned that the fatigue limit is primarily governed by two factors<sup>14–17</sup>. The initial factor is the stress concentration induced by notches. H. Neuber<sup>18</sup> introduced the average stress model to predict the notch

<sup>1</sup>Jiangsu Province Key Laboratory of Aerospace Power System, College of Energy and Power Engineering, Nanjing University of Aeronautics and Astronautics, Nanjing 210000, China. <sup>2</sup>Fundamentals Department, Air Force Engineering University, Xi'an 710051, China. <sup>3</sup>National Key Lab of Aerospace Power System and Plasma Technology, Air Force Engineering University, Xi'an 710038, China. <sup>4</sup>Jiangsu Aero-XY Technology Co., Ltd, Wuxi 214000, China. <sup>5</sup>State Key Laboratory of Mechanics and Control for Aerospace Structures, Nanjing University of Aeronautics and Astronautics, Nanjing 210000, China. ✉email: ableshang@163.com; zhaozhenhua@nuaa.edu.cn; happyzlch@163.com

fatigue strength and devised the Neuber formula for determining the notch fatigue coefficient. Peterson<sup>19</sup> further refined the average stress model, proposing a simplified version of Peterson's formula, which is widely adopted in engineering practices. Ruschau<sup>20</sup> used the aforementioned empirical formula for fatigue notch coefficient to predict the high-cycle fatigue strength of damaged TC4 material specimens. It was found that the predicted results derived from the empirical formula were relatively high. Weibull<sup>21</sup> developed the weakest cycle theory based on the statistical analysis. This theory posits that the underlying cause of component failure is the breakdown of specific geometric dimensions under the influence of internal material forces and external loads. Zhang H<sup>22,23</sup> carried out laboratory simulated FOD tests by air gun. The effect of the initial stress state and impact position on FOD was investigated by numerical prediction. Additionally, FOD prediction models about impact velocity and impact energy were developed using the linear and power formulas, respectively. The predicted results could serve as the upper and lower bounds within the damage space to envelope the test results, providing a reference for fatigue life assessment of the aeroengine blades.

The second factor involves the influence of local stress/strain field within the notch. Taylor<sup>24</sup> proposed the theory of critical distances (TCD) to predict notch fatigue limits. This theory assesses the average stress within a localized area of the cross-section at the notch root. Yamashita<sup>25</sup> used the critical distance theory to predict the fatigue strength of micro-notched specimens. A good correlation exists between the critical distance stress and fatigue life of small-notched specimens if the critical distance is calibrated by the two notched fatigue failure curves of specimens with different notch root radii. Benedetti et al.<sup>26</sup> used the line method of critical distance theory to predict the notch fatigue strength of shot-peened Al-7075-T651 material flat specimens. The TCD demonstrates relative accuracy when predicting the notch fatigue specimens under residual compressive stress fields. Hudak<sup>27</sup> proposed a worst-case notch model to predict high-cycle fatigue in damaged components. This model posits that microcracks initiated at the damage root during the initial fatigue loading stage, enabling prediction of the high-cycle fatigue strength of damaged components based on the crack propagation boundary conditions. Nowell<sup>28</sup> used a short crack arrest model which is akin to the worst-notch theory to predict the high-cycle fatigue strength of FOD notch specimens. The primary factor influencing the prediction accuracy is that the model neglected the influence of residual compressive stress at the damage root. Chaves et al.<sup>29</sup> proposed a method based on the microstructure fracture mechanics model (Navarro, 1988<sup>30</sup>) for predicting fatigue limits under remote loading via stress gradient and linear elastic analysis. The circular holes and V-shaped notches under I-type loads showed that the prediction errors are within 12%.

Based on the literature survey summarized above, it can be found that it's a challenging but necessary work to build more accurate models for predicting the high cycle fatigue limit of foreign object damaged blades. In this paper, machining aerofoil specimens were manufactured to simulate the foreign object damaged blade, and the high cycle fatigue limit of machining foreign object damaged TC17 titanium aerofoil specimen were tested at  $3 \times 10^7$  cycles, and a high cycle fatigue limit prediction model of machining foreign object damaged TC17 titanium aerofoil specimen was built based on the theory of critical distances, and compared with the Peterson model.

## Experimental procedures

### Material and specimen

The material used in the present work is TC17 titanium alloy, which is a typical  $\alpha + \beta$  two phase titanium alloy with near  $\beta$  mutually. The nominal composition of the material is Ti-5Al-2Sn-2Zr-4Mo-4Cr. The material properties at room temperature are as follows: the density is 4680 kg/m<sup>3</sup>, the elastic modulus is 112.0GPa, the Poisson's ratio is 0.301, the tensile strength is 1120 MPa and the bending fatigue strength of  $R = -1$  is 440 MPa.

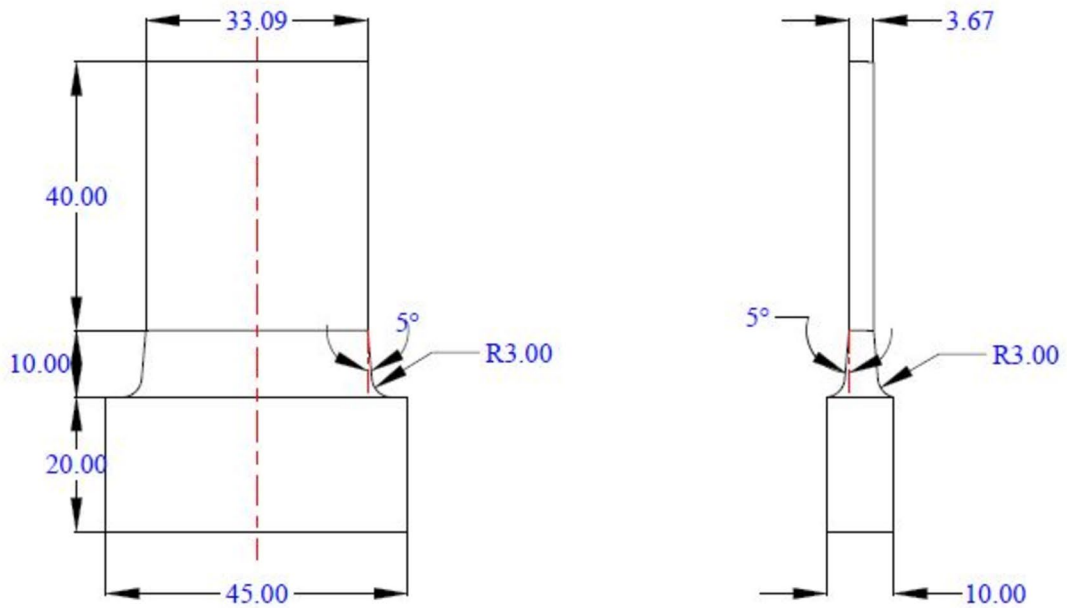
To simulate the characteristics of aero-engine compressor blades' leading edge, the specimen is designed as an aerofoil specimen. The specimen dimension and specimen entity are shown in (Figs. 1, 2), respectively.

### Machining of notches

To investigate the influence of machining notch size parameters on the fatigue performance, the specimens were mechanically machined. The shape and machining position of the notch are shown in (Figs. 3, 4), respectively. The normal line of the notch plane is perpendicular to the neutral surface of the leading edge of the specimen. The machining size of the notch is shown in (Table 1). The laser confocal scanning microscope (LEXT OLS5000) was used to measure the surface roughness of the machined notch.

To investigate the stress intensity factor of the notched blade, the first-order bending mode vibration was simulated with the complete blade and the notched blade. The model was meshed with tetrahedral grids by Altair Hypermesh 14.0. The mesh size of the whole structure is 0.3 mm, and the mesh size near the notch is 0.1 mm. The meshes of the complete specimen and the machined notch specimen are shown in (Fig. 5a,b), respectively. The constraints were imposed on both sides of the clamping end, limiting all degrees of freedom. The calculated results of stress distribution of the first-order bending mode are shown in (Fig. 6).

The maximum stress around the notch (corresponding to the dangerous point)  $\sigma_{\max}$  of the notched specimen and the stress  $\sigma_0$  of the same position of complete specimen are extracted. The maximum displacement of the blade tip  $S_{\max}$  (for notched specimen) and  $S_0$  (the same position for the complete specimen) are also extracted. Typically, the stress concentration factor  $K_t$  is calculated as the ratio of  $\sigma_{\max}$  and  $\sigma_0$ , i.e.  $K_t = \sigma_{\max}/\sigma_0$ . However, this equation derives from the prerequisite that the far-field displacement  $S_0$  (or stress  $\sigma_{\text{far}}$ ) of the complete specimen and the far-field displacement  $S_{\max}$  (or stress  $\sigma'_{\text{far}}$ ) of the notched specimen are consistent. Otherwise, the influence of far-field stress or displacement inconsistency should be considered, and the  $K_t$  should be multiplied by the corresponding proportional coefficient  $S_0/S_{\max}$  or  $\sigma_{\text{far}}/\sigma'_{\text{far}}$ . This approach is typically used in the vibration fatigue experiment of notched blade<sup>31,32</sup>. Therefore, the stress concentration factor  $K_t$  of the notch is obtained by Eq. (1):



4:1

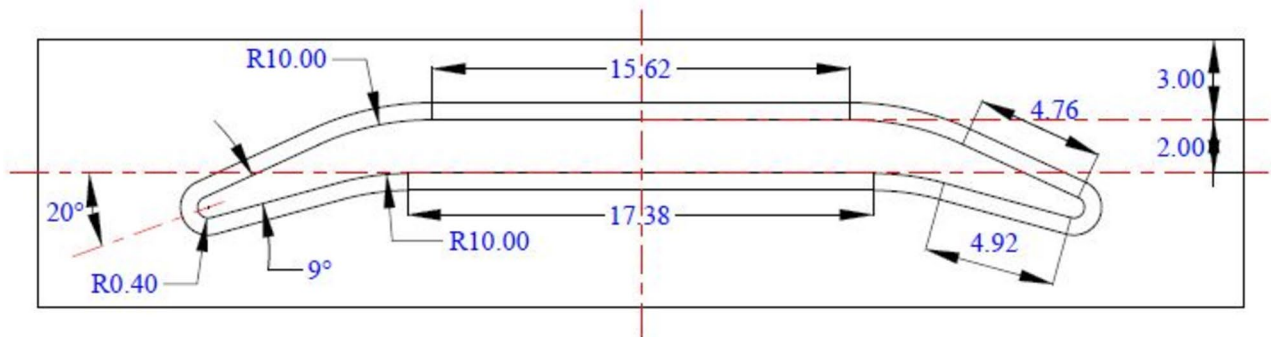


Fig. 1. Specimen dimension (all dimensions are in millimeters).

$$K_t = \frac{\sigma_{\max}}{S_{\max}} \times \frac{S_0}{\sigma_0} \tag{1}$$

The stress concentration factor  $K_t$  calculated by finite element method is shown in (Table 1).

**High cycle fatigue tests**

High cycle fatigue (HCF) tests of machined notched specimens were carried out on a vibration table with a dedicated fixture. The fixture is divided into three parts: the pressure block, the top block, and the base. The base is connected to the vibration table base via M12 bolts, while the pressure block is connected to the base using M14 bolts to clamp the holding section of the simulated blade. The fixture is made of 45# steel, which provides sufficient stiffness. Additionally, larger-sized bolts are used in the design to ensure adequate preload, preventing any changes in boundary conditions due to loosening during the test. The load of vibration table is feedback controlled by an accelerometer. The vibration status of specimen was real-time monitored through a strain gauge and the target strain amplitude was maintained by adjusting the load of vibration table. Figure 7 shows the clamping method of specimen and the position of strain gauge.

Based on the stress calculation results in Part 2.2, the relationship between nominal stress and strain measurement positions of different notch depths was established. In the HCF test, the strain data was collected

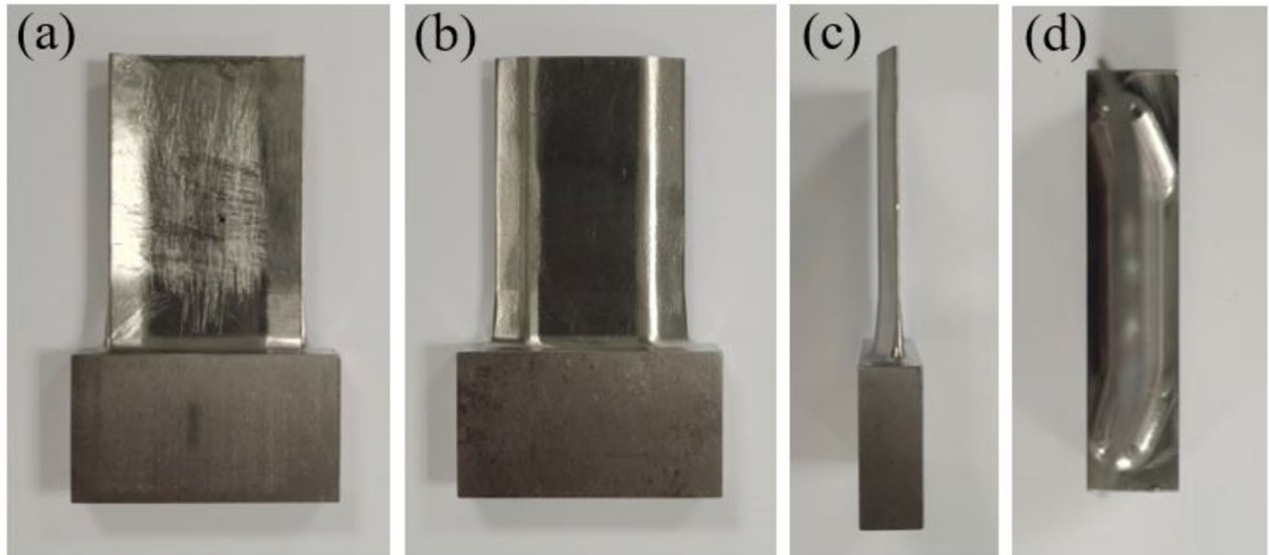


**Fig. 2.** The manufactured specimen (a) front view (b) rear view (c) left view (d) vertical view.

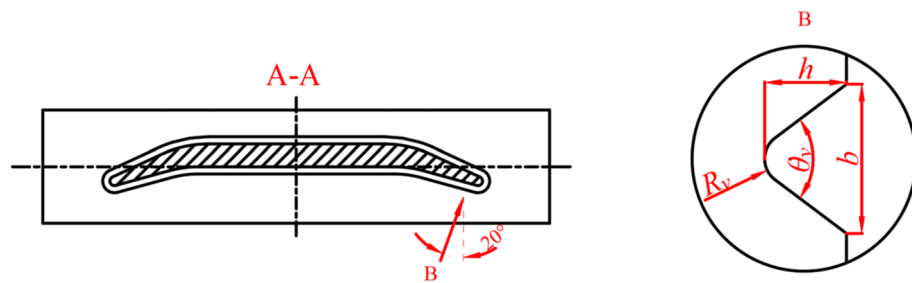


**Fig. 3.** The shape of notch.

and saved in real-time using a strain gauge, and the nominal stress at the root of the notch is calculated. The fatigue limit of the specimen is determined at the time of fatigue failure<sup>33</sup>.

HCF tests were carried out by “step-loading method” (Maxwell and Nicholas<sup>34</sup>, 1999), and the fatigue limit at  $3 \times 10^7$  cycles was evaluated experimentally. In this method, if a given specimen survives at the initial stress level, the stress level should be increased by 10% of the initial value and then the test repeats. This process continued until the specimen failed in less than  $3 \times 10^7$  cycles. The load spectrum for one of specimen in notch type I is shown in the Fig. 8 as an example. For specimens of different notch types, the initial stress level should be changed appropriately.

Assume that the fatigue damage accumulates linearly in the last step of loading, the fatigue limit at  $3 \times 10^7$  cycles can be calculated by the following equation<sup>33</sup>:

$$\sigma_e = \sigma_p + \frac{n}{3 \times 10^7} \times (\sigma_f - \sigma_p) \quad (2)$$

where  $\sigma_e$  is the fatigue strength of specimen at  $3 \times 10^7$  cycles,  $\sigma_p$  is the stress level before fatigue failure occurs in specimen,  $\sigma_f$  is the stress level at which fatigue failure occurs in specimen, and  $n$  is the number of cycles when fatigue failure occurs. In the present work, 9 specimens of various dimensions were HCF tested, and the specimen number is shown in (Table 1). After the HCF tests, the scanning electron microscope (Zeiss Sigma 300) was used to characterize the fatigue fracture surface of the machined notch.

## Experimental results

### Surface roughness

Figure 9 showed the surface profile measurement results of three types of machined notches. The arithmetic mean deviation ( $S_a$ ) of the contours of three machined notches with depths of 0.5, 1, and 1.5 mm are 23.908, 16.632, and 17.433  $\mu\text{m}$ , respectively. The arithmetic mean deviations  $S_a$  of the contours of three machined notches with depth of 1 mm and width of 1.62 mm are 17.464 $\mu\text{m}$ , 21.319 $\mu\text{m}$  and 23.119 $\mu\text{m}$ , respectively. The

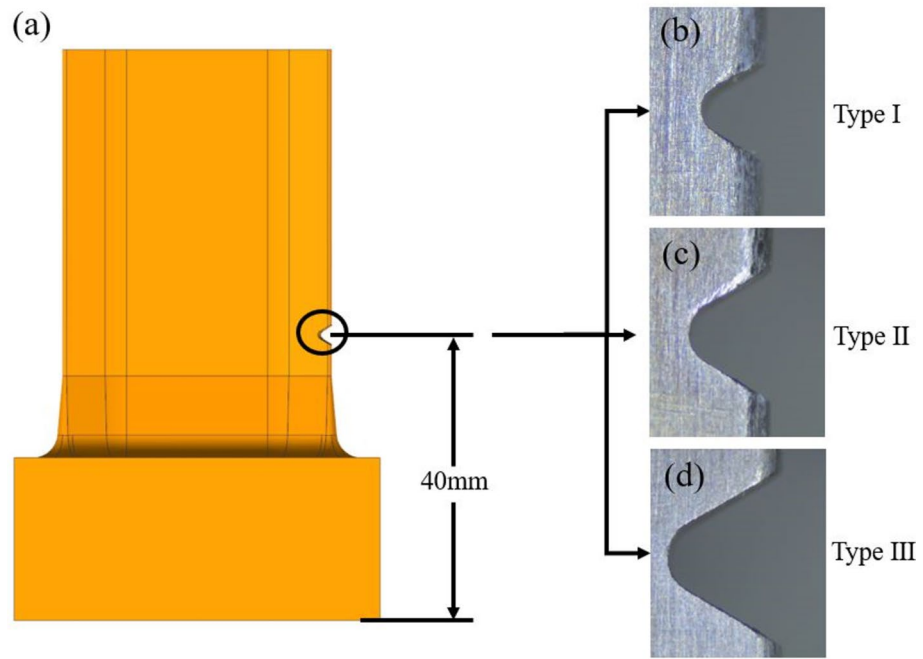


**Fig. 4.** The position and type of notch (a) the notch position (b) notch type I (c) notch type II (d) notch type III.

Notch type	Specimen number	Flare angle $\theta_v/^\circ$	Depth $h/\text{mm}$	Width $b/\text{mm}$	Bottom radius $R_v/\text{mm}$	Stress concentration factor $K_t$
I	I-1	60	0.5	0.8	0.2	3.06
	I-2					
	I-3					
II	II-1	60	1	1.62	0.4	3.10
	II-2					
	II-3					
III	III-1	60	1.5	2.31	0.5	3.28
	III-2					
	III-3					

**Table 1.** The machining size of notch.

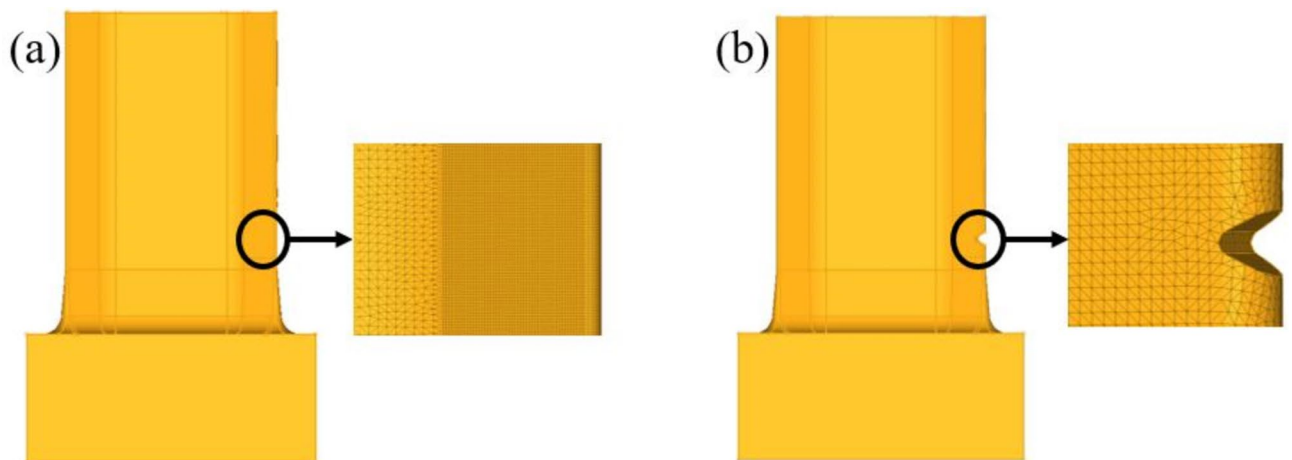


**Fig. 5.** The mesh of aerofoil specimen (a) the complete specimen (b) the notched specimen.

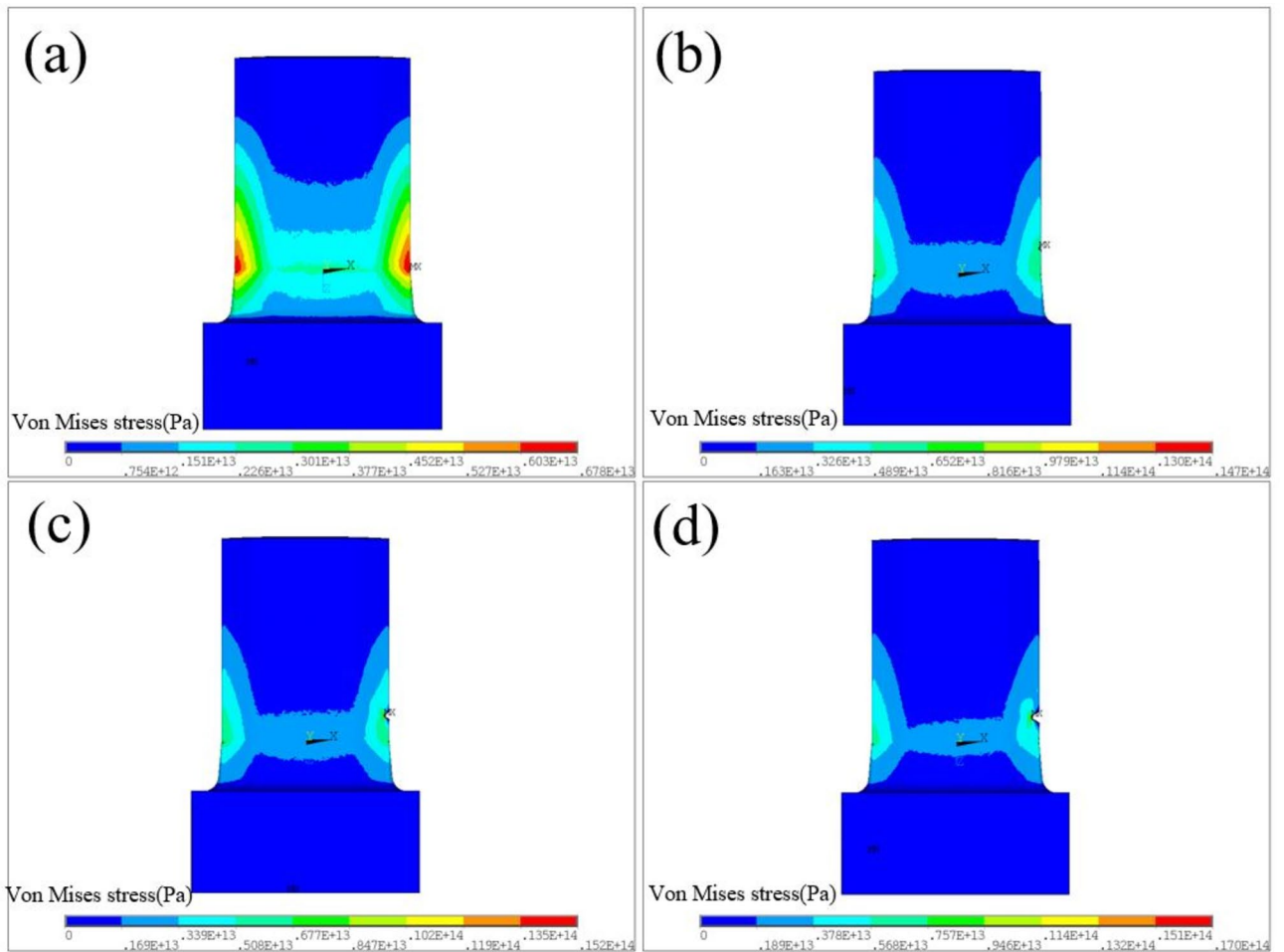


**Fig. 6.** The mesh of aerofoil specimen (a) the complete specimen (b) the notched specimen of type I (c) the notched specimen of type II (d) the notched specimen of type III.

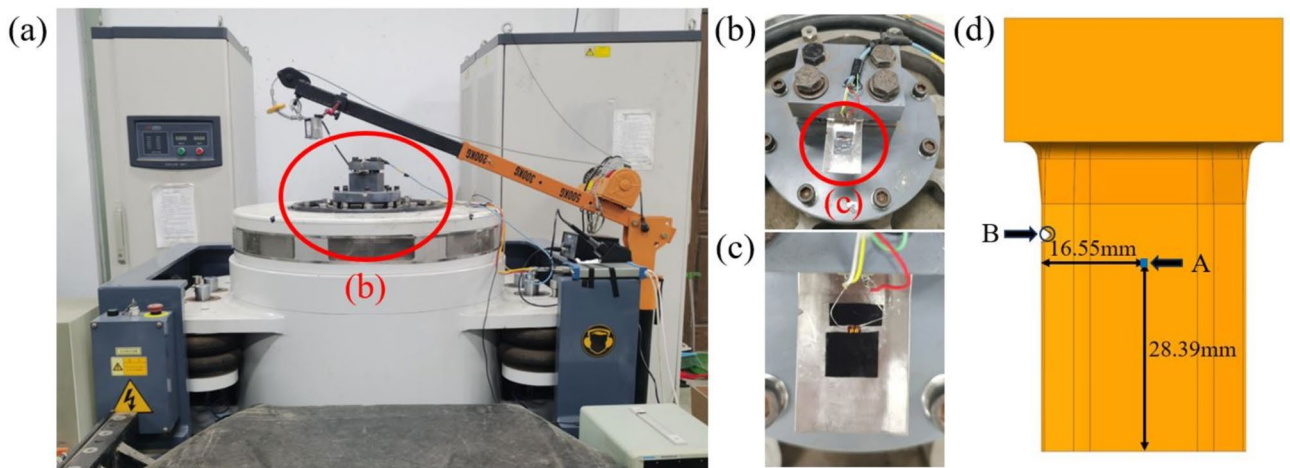


**Fig. 7.** The HCF test (a) vibration test bench (b) the fixture (c) the strain gauge location (d) the strain gauge.

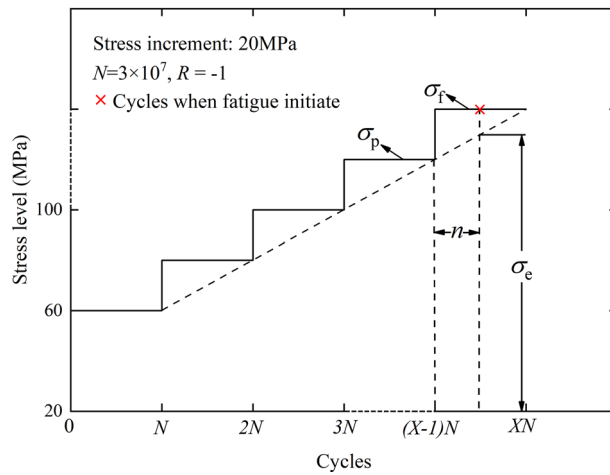


Fig. 8. The load spectrum for HCF tests.

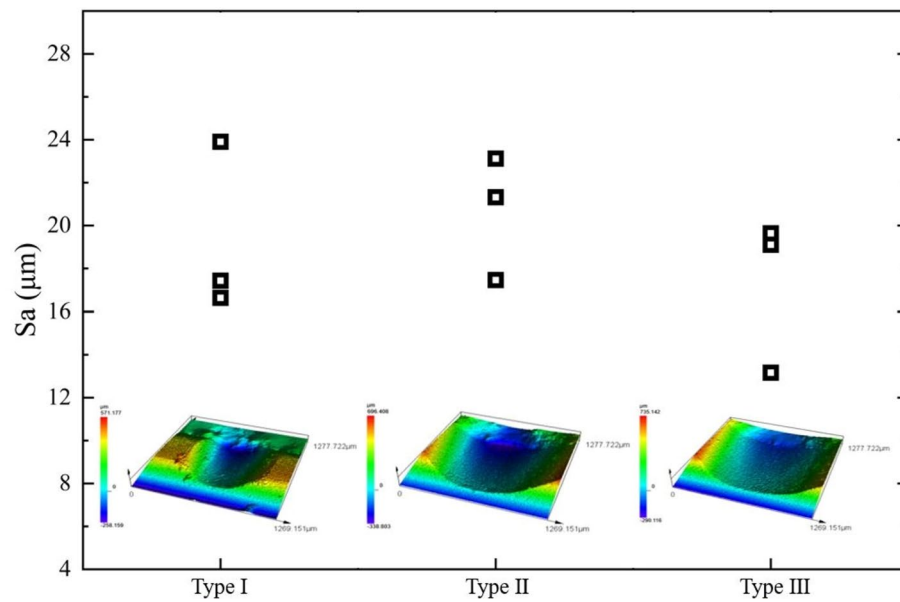


Fig. 9. The surface roughness measurement results.

arithmetic mean deviations  $S_a$  of the contours of three machined notches with depth of 1.5 mm and width of 2.31 mm are 13.161 $\mu\text{m}$ , 19.106 $\mu\text{m}$  and 19.638 $\mu\text{m}$ , respectively.

### Fatigue limit

In the high cycle fatigue test, the stress of notch root (the damaged position with maximum stress) is calculated according to the strain of the strain measurement point by the following equation<sup>33</sup>:

$$\sigma_{B\_Test} = E\varepsilon_{A'} \cdot \frac{\sigma_{B\_Simu}}{\sigma_{A\_Simu}} \quad (3)$$

where  $\sigma_{A\_Simu}$  is the Mises stress of strain measurement point (point A) in finite element simulation results of first order bending mode analysis with un-notched aerofoil sample,  $\sigma_{B\_Simu}$  is the Mises stress of notch root (the damaged position with maximum stress, point B) in finite element simulation results of first order bending mode analysis with un-notched aerofoil sample,  $\varepsilon_{A'}$  is the strain measured at the strain measurement point in the test,  $E$  is the elastic modulus of TC17.

The HCF limit of the machined notch specimen at  $3 \times 10^7$  cycles was shown in (Fig. 10). The high cycle fatigue limit of machined notch specimens with different sizes has a large dispersion. With the increase of stress concentration factor  $K_t$ , the HCF fatigue limit of the machined notch specimen was reduced significantly.

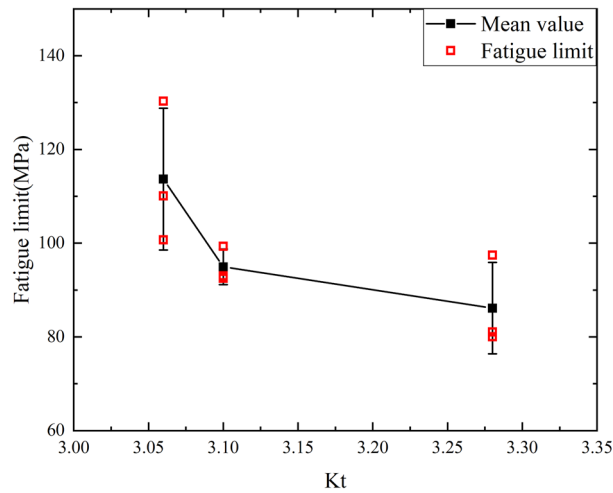


Fig. 10. The HCF limit tested.

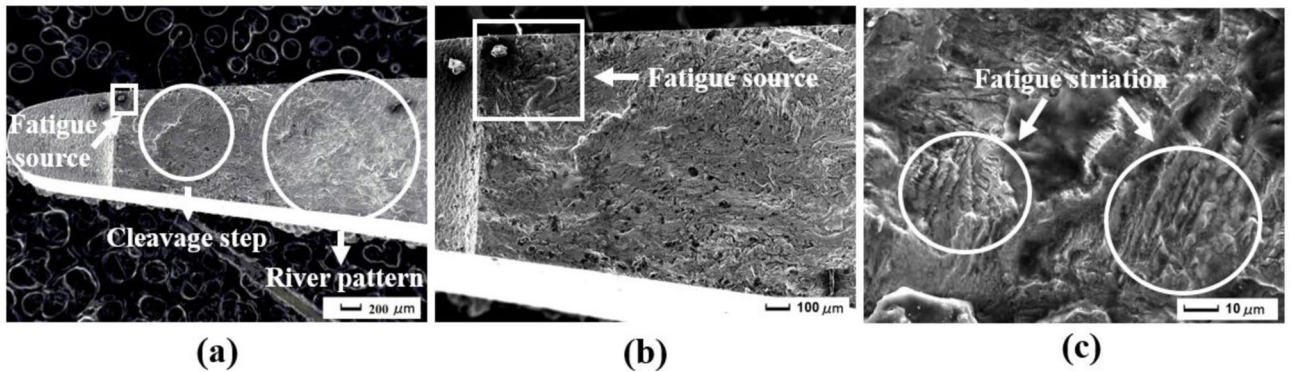


Fig. 11. Schematic diagram of fatigue limit prediction model based on TCD. (a) The overall morphology of the fracture surface. (b) Fatigue source. (c) Fatigue striation.

### Fatigue strength prediction model TCD model

#### Model building process

According to the theory of critical distances (TCD), the fatigue strength can be predicted by the hot spot stresses within a certain range in front of crack tip. In our previous work<sup>35</sup>, a model based on the TCD method was built to predict the fatigue strength of FOD notched blades. Considering integrity of the paper, the model building process was presented here. The model construction process was shown in (Fig. 11).

According to the volume method of TCD, the average stress within the region near critical point B (i.e., the region within the hemispherical domain along the notch depth direction with point B as the hemisphere center and the critical distance  $r_c$  as the hemisphere radius),  $\sigma_{aver_0}$ , is equal to the fatigue limit of smooth specimen  $\sigma_{-1}$ , namely  $\sigma_{aver_0} = \sigma_{-1}$ . Similar first-order bending vibration mode analysis can also be carried out by numerical simulation. Therefore, the following relationship can be reached:

$$\frac{\sigma_{A'}}{\sigma_{-1}} = \frac{\sigma_{A'}}{\sigma_{aver_0}} = \frac{\sigma_{A'}_{Simu}}{\sigma_{aver_{Simu}}} \tag{4}$$

where  $\sigma_{A'_{Simu}}$  and  $\sigma_{aver_{Simu}}$  are the stresses of corresponding positions calculated by numerical simulation, respectively. Multiply both sides of Eq. (4) by  $\sigma_{B_{Simu}}/\sigma_{A_{Simu}}$ :

$$\frac{\sigma_{A'}}{\sigma_{-1}} \cdot \frac{\sigma_{B_{Simu}}}{\sigma_{A_{Simu}}} = \frac{\sigma_{A'}_{Simu}}{\sigma_{aver_{Simu}}} \cdot \frac{\sigma_{B_{Simu}}}{\sigma_{A_{Simu}}} \tag{5}$$

Substitute Eq. (3) into Eq. (5):

$$\frac{\sigma_{B_{Test}}}{\sigma_{-1}} = \frac{\sigma_{A'}_{Simu}}{\sigma_{aver_{Simu}}} \cdot \frac{\sigma_{B_{Simu}}}{\sigma_{A_{Simu}}} \tag{6}$$

In Eq. (6),  $\sigma_{B\_Test}$  is obtained from Eq. (3) with the first-order bending vibration fatigue experiment,  $\sigma_{-1}$  is the material parameter and can be obtained from the material manual,  $\sigma_{A\_Simu}$  and  $\sigma_{aver\_Simu}$  are obtained from the numerical simulation of first-order bending vibration mode analysis of notched sample,  $\sigma_{A\_Simu}$  and  $\sigma_{B\_Simu}$  are obtained from the numerical simulation of first-order bending vibration mode analysis of un-notched sample.

#### Model application

Equation (6) can be used for the critical distance calculation or bending vibration fatigue strength prediction with the following method:

- (I) To calculate the critical distance  $r_c$ , the first-order bending vibration fatigue experiment and the numerical simulation of first-order bending vibration mode analysis was conducted on both the notched blade and the un-notched blade. With  $\sigma_{B\_Test}$ ,  $\sigma_{-1}$ ,  $\sigma_{A\_Simu}$ ,  $\sigma_{A\_Simu}$  and  $\sigma_{B\_Simu}$  already known, the critical distance  $r_c$  which matches Eq. (6) can be calculated by numerical iteration.
- (II) To predict the bending vibration fatigue strength, the critical distance  $r_c$  was already known, and the numerical simulation of first-order bending vibration mode analysis was conducted on both the notched blade and the un-notched blade. With  $\sigma_{-1}$ ,  $\sigma_{A\_Simu}$ ,  $\sigma_{aver\_Simu}$ ,  $\sigma_{A\_Simu}$  and  $\sigma_{B\_Simu}$  already known, the predicted  $\sigma_{B\_Test}$  can be calculated as  $\sigma_{B\_Predicted}$  with Eq. (6) and validated by comparison with the experimental result  $\sigma_{B\_Test}$ .

#### Peterson model

Peterson model is one of the most widely used models for predicting the fatigue strength of notched components in engineering, which can be described by the following equation<sup>36</sup>:

$$K_f = 1 + \frac{K_t - 1}{1 + a_p/\rho} \quad (7)$$

where  $K_t$  is the stress concentration factor,  $\rho$  is the radius of the notch root,  $a_p$  is the material constant influenced by tensile strength. In the present work, the stress concentration factor  $K_t$  is calculated by numerical simulation with the Eq. (1), and  $a_p$  (Unit: MPa) is calculated with the following equation<sup>37</sup>:

$$a_p = 0.0254 \left( \frac{2070 \text{ MPa}}{\sigma_u} \right)^{1.8} \quad (8)$$

where  $\sigma_u$  is the tensile strength (Unit: MPa). In the present work,  $a_p = 0.07673$  mm. After getting the fatigue notch factor  $K_f$  by Eq. (8), the fatigue limit of notched sample  $\sigma_{-1}/K_f$  can be calculated using  $\sigma_{-1}$  of TC17 at  $3 \times 10^7$  cycles. In the present work,  $\sigma_{-1} = 440$  MPa.

### Fatigue strength prediction

#### Fatigue strength prediction based on the TCD method

First-order bending vibration fatigue experiments were carried out with 3 notched aerofoil specimens of various notch dimensions (specimen No. I-2/II-1/III-1). For details of the experiment procedure, please tend to Part 2 and Part 3 of this paper. The fatigue strength of notched aerofoil sample  $\sigma_{B\_Test}$  was calculated with Eq. (6) for each specimen.

First-order bending vibration mode analysis of the un-notched aerofoil sample and 3 notched aerofoil sample of various notch dimensions (specimen No. I-2/II-1/III-1) were carried out by numerical simulation. For details of the numerical simulation procedure, please tend to Part 2 of this paper. FEM models of the un-notched and notched aerofoil specimen for bending vibration mode analysis were also shown in (Fig. 11). The Mises stress and the normal stress along the aerofoil specimen length direction at point A, the Mises stress at point B, and the node position coordinate, element volume and the principal stress of each node around the point B were calculated. Therefore, the  $\sigma_{A\_Simu}$ ,  $\sigma_{A\_Simu}$  and  $\sigma_{B\_Simu}$  in Eq. (6) can be obtained directly.

In Eq. (6),  $\sigma_{aver\_Simu}$  is the average stress of the region near point B (i.e., the region within the hemispherical domain along the notch depth direction with point B as the hemisphere center and the critical distance  $r_c$  as the hemisphere radius) in numerical simulation of the notched aerofoil specimen, and can be calculated as:

$$\sigma_{aver\_Simu} = \eta \frac{\sum_{i=1}^N \sigma_i \cdot V_i}{\sum_{i=1}^N V_i} \quad (9)$$

where  $N$  is the number of elements whose gravity center is within the proposed hemisphere domain,  $\sigma_i$  is the maximum absolute value of the principal stress of element,  $V_i$  is the volume of element,  $\eta$  is the correction factor for bending effect and  $\eta = 4$  in the present work.

The  $\sigma_{B\_Test}$ ,  $\sigma_{A\_Simu}$ ,  $\sigma_{A\_Simu}$  and  $\sigma_{B\_Simu}$  have been obtained in Part 3.2, and  $\sigma_{-1} = 440$  MPa of TC17 material was used here. Therefore, the critical distance  $r_c$  can be calculated by numerical interaction with Eq. (6) for each notched blade specimen. For simplicity, the critical distance  $r_c$  is supposed to be a constant material parameter in the present work. The average value of the critical distance  $r_c$  for the 3 specimens is  $r_c = 0.7075$  mm. The critical distance  $r_c$  of each specimen is shown in (Table 2).

Notch type	The von Mises stress at point A of the complete blade (MPa)	The von Mises stress at point B of the complete blade (MPa)	The von Mises stress at point A of the notched blade (MPa)	The principal stress of each node around the point A of the notched blade (MPa)	Modal von Mises stress at point B of the notched blade (MPa)	Critical distance $r_c$ /mm
I	68.3	324.877	67.925	74.943	994.74	0.6525
II		306.453	67.866	74.744	969.281	0.7425
III		287.985	69.214	76.188	994.427	0.7275

**Table 2.** The critical distance  $r_c$  of each specimen.

Notch type	Specimen number	Tested fatigue strength/MPa	Fatigue strength prediction			
			TCD model		Peterson model	
			Predicted fatigue strength/MPa	Error (%)	Predicted fatigue strength/MPa	Error (%)
I	I-1	100.67	113.82	13.06	175.83	74.66
	I-3	130.27	113.82	12.63	175.83	34.98
II	II-2	99.33	90.30	9.09	155.38	56.43
	II-3	92.50	90.30	2.37	155.38	67.98
III	III-2	97.40	78.97	18.92	142.53	46.33
	III-3	80.00	78.97	1.29	142.53	78.16

**Table 3.** Fatigue strength prediction results.

### Fatigue strength prediction results

To validate the accuracy of the TCD model, another 6 notched blades of various notch dimensions (specimen No. I-1/I-3/II-2/II-3/III-2/III-3) were HCF tested, and the predicted fatigue strength  $\sigma_{B\_Predicted}$  were compared with the experimental test results  $\sigma_{B\_Test}$ . The first-order bending vibration fatigue experiments were carried out and the fatigue strength  $\sigma_{B\_Test}$  was calculated with Eq. (3) for each specimen. Numerical simulation of the first-order bending vibration mode analysis was carried out, and  $\sigma_{A\_Simu}$  and  $\sigma_{aver\_Simu}$  can be obtained with  $\eta = 4$  and  $r_c = 0.7075$  mm. Un-notched blades were also used for numerical simulation of the first-order bending vibration mode analysis, and  $\sigma_{A\_Simu}$  and  $\sigma_{B\_Simu}$  can be obtained. Therefore, the predicted  $\sigma_{B\_Test}$  can be calculated as  $\sigma_{B\_Predicted}$  with Eq. (6), where  $\sigma_{-1} = 440$  MPa.

Peterson model was also used to predict the fatigue limit of these 6 notched samples. Table 3 and Fig. 12 showed the comparison between the predicted fatigue strength  $\sigma_{B\_Predicted}$  and the tested results  $\sigma_{B\_Test}$ . The prediction error is  $9.56\% \pm 6.78\%$  for TCD model and  $59.76\% \pm 16.93\%$  for Peterson model (Fig. 13). The accuracy of fatigue limit prediction on notched samples using TCD model is much higher than that of Peterson model. It can be concluded that the TCD method model is more efficient to evaluate the fatigue strength of notched blade.

### Conclusion

In the present work, comprehensive investigation of machining foreign object damage effect on the fatigue limit of TC17 aerofoil specimen and high cycle fatigue limit prediction of machining foreign object damaged titanium aerofoil specimen were carried out. The following conclusions can be reached:

- (1) Machining notch can be used for foreign object damage analysis, and the machined notch dimension and surface roughness can influence the high cycle fatigue limit of the TC17 titanium aerofoil specimen. The high cycle fatigue limit of machined notch specimens with different sizes has a large dispersion. With the increase of stress concentration factor  $K_t$ , the HCF fatigue limit of the machined notch specimen reduced significantly.
- (2) The model based on the TCD method can be used for fatigue strength prediction of notched blades in first-order bending vibration mode. The prediction error is  $9.56\% \pm 6.78\%$  for TCD model and  $59.76\% \pm 16.93\%$  for Peterson model. The accuracy of fatigue limit prediction on notched samples using TCD model is much higher than that of Peterson model, and the TCD method model is more efficient to evaluate the fatigue strength of notched blade.

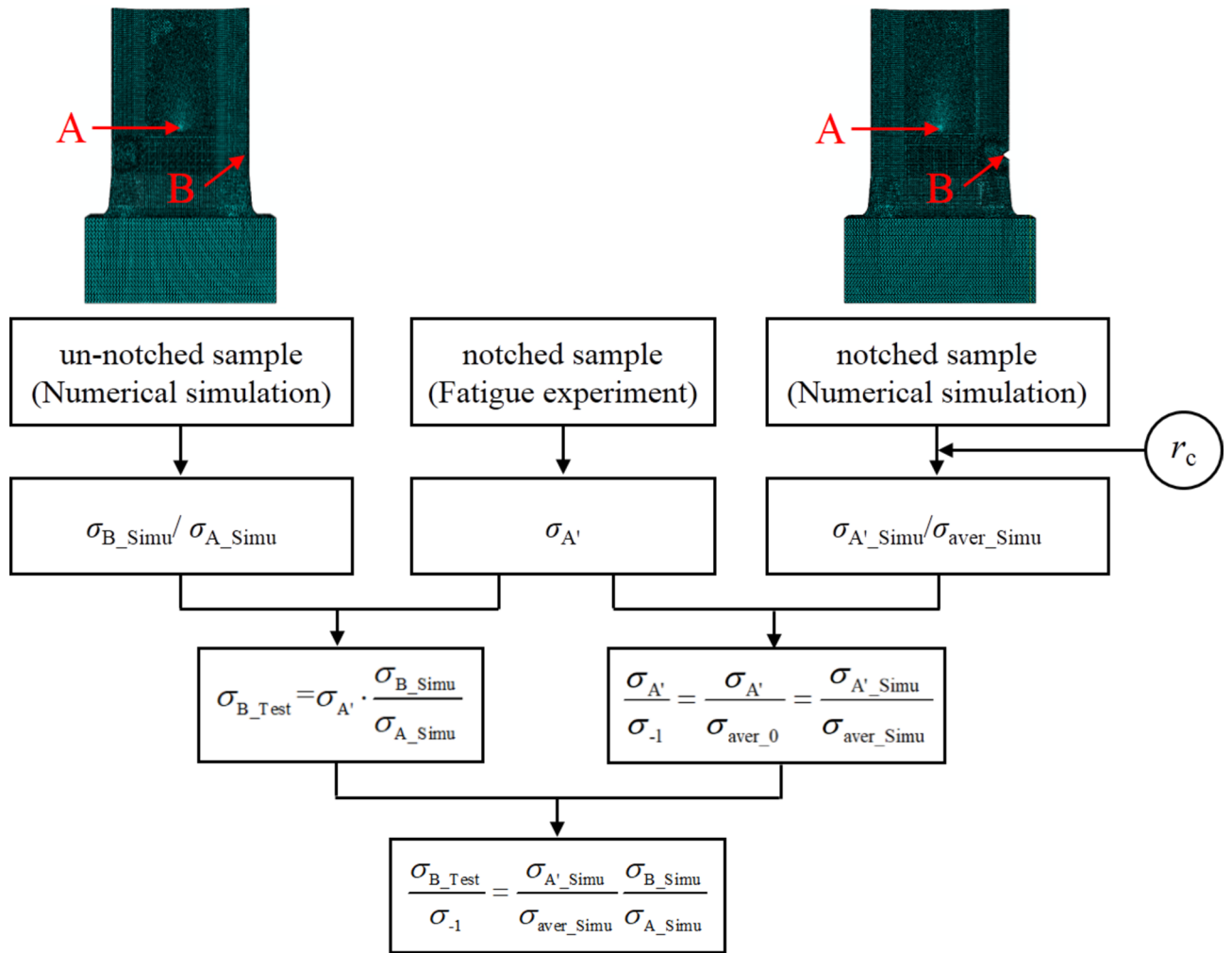
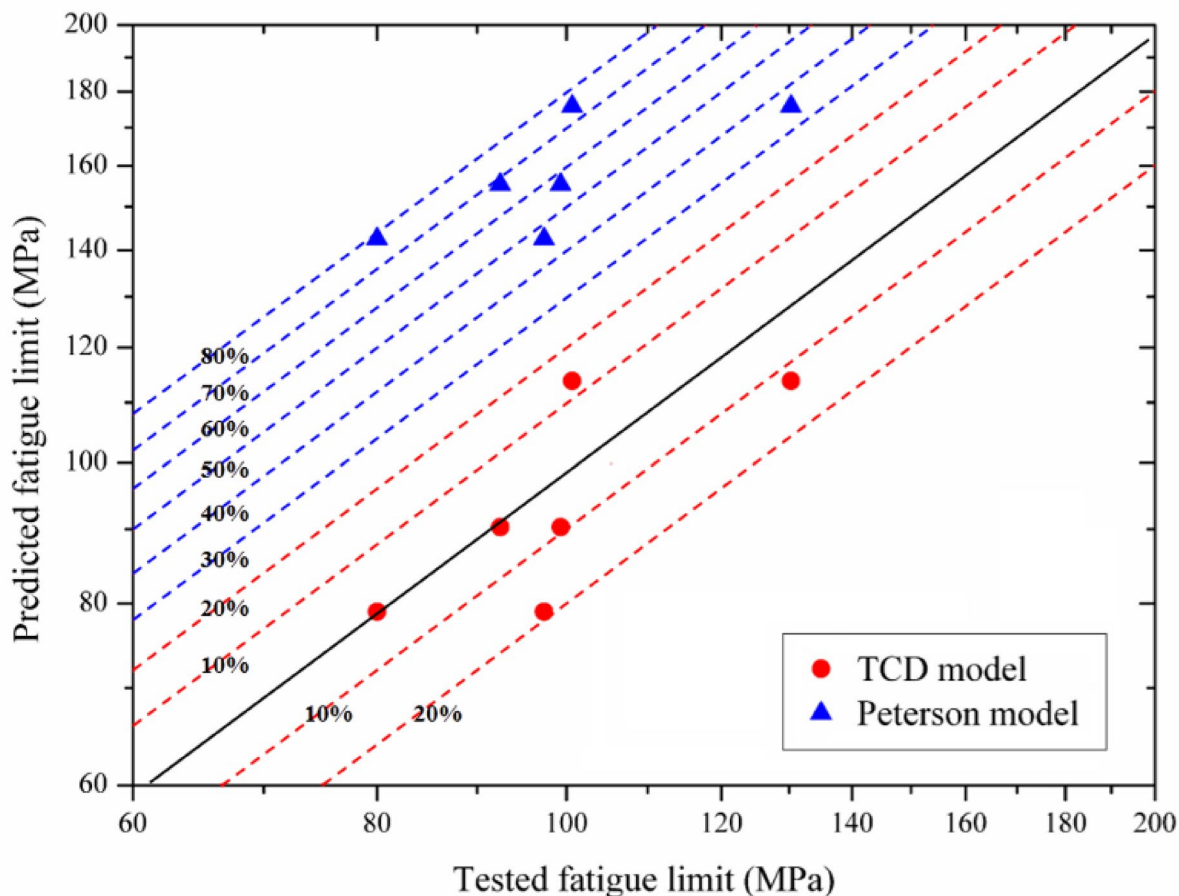


Fig. 12. Comparison of the predicted results with the test results for different models.



**Fig. 13.** Comparison of fatigue limit prediction results by TCD model and Peterson model

### Data availability

The raw/processed data required to reproduce these findings cannot be shared at this time as the data also forms part of an ongoing study. Data requests can be made to Lu Kainan via this email: lukainan@nuaa.edu.cn.

Received: 22 October 2024; Accepted: 20 May 2025

Published online: 04 June 2025

### References

- Nicholas, T. Critical issues in high cycle fatigue. *Int. J. Fatigue* **21**, S221–S231. [https://doi.org/10.1016/S0142-1123\(99\)00074-2](https://doi.org/10.1016/S0142-1123(99)00074-2) (1999).
- Xi, C. Foreign object damage on the leading edge of a thin blade. *Mech. Mater.* **37**(4), 447–457. <https://doi.org/10.1016/j.mechmat.2004.03.005> (2005).
- Sharma, R., Singh, S. & Singh, A. K. Foreign object damage investigation of a bypass vane of an aero-engine. *Mater. Today: Proc.* **5**(9), 17717–17724. <https://doi.org/10.1016/j.matpr.2018.06.094> (2018).
- Spanrad, S. & Tong, J. Characterisation of foreign object damage (FOD) and early fatigue crack growth in laser shock peened Ti-6Al-4V aerofoil specimens. *Mater. Sci. Eng. A* **528**(4–5), 2128–2136. <https://doi.org/10.1016/j.msea.2010.11.045> (2010).
- Han, L. et al. Probability-based service safety life prediction approach of raw and treated turbine blades regarding combined cycle fatigue. *Aerosp. Sci. Technol.* **110**, 106513. <https://doi.org/10.1016/j.ast.2021.106513> (2021).
- Ruschau, J. J., Nicholas, T. & Thompson, S. R. Influence of foreign object damage (FOD) on the fatigue life of simulated Ti-6Al-4V airfoils. *Int. J. Impact. Eng.* **25**(3), 233–250. [https://doi.org/10.1016/S0734-743X\(00\)00044-0](https://doi.org/10.1016/S0734-743X(00)00044-0) (2001).
- Mall, S. & Hamrick, J. L. High cycle fatigue behavior of Ti-6Al-4V with simulated foreign object damage. *Mech. Mater.* **33**(11), 679–692. [https://doi.org/10.1016/S0167-6636\(01\)00084-9](https://doi.org/10.1016/S0167-6636(01)00084-9) (2001).
- Cowles, B. A. High cycle fatigue in aircraft gas turbines—An industry perspective. *Int. J. Fract.* **80**, 147–163. <https://doi.org/10.107/BF00012667> (1996).
- Coles, A. Damage to axial compressors. *Aeronaut. J.* **63**(588), 731–731. <https://doi.org/10.1017/S000192400093349> (1959).
- Nicholas, T. *High Cycle Fatigue: A Mechanics of Materials Perspective* (Elsevier, 2006).
- Ruschau, J. J., John, R., Thompson, S. R. & Nicholas, T. Fatigue crack nucleation and growth rate behavior of laser shock peened titanium. *Int. J. Fatigue* **21**, S199–S209. [https://doi.org/10.1016/S0142-1123\(99\)00072-9](https://doi.org/10.1016/S0142-1123(99)00072-9) (1999).
- Nowell, D., Duo, P. & Stewart, I. F. Prediction of fatigue performance in gas turbine blades after foreign object damage. *Int. J. Fatigue* **25**, 963–969. [https://doi.org/10.1016/S0142-1123\(03\)00160-9](https://doi.org/10.1016/S0142-1123(03)00160-9) (2003).

13. Nicholas, T., Thompson, S. R., Porter, W. J. & Buchanan, D. J. Comparison of fatigue limit strength of Ti-6Al-4V in tension and torsion after real and simulated foreign object damage. *Int. J. Fatigue* **27**(10–12), 1637–1643. <https://doi.org/10.1016/j.ijfatigue.2005.06.012> (2005).
14. Thompson, S. R., Ruschau, J. J. & Nicholas, T. Influence of residual stresses on high cycle fatigue strength of Ti-6Al-4V subjected to foreign object damage. *Int. J. Fatigue* **23**, 405–412. [https://doi.org/10.1016/S0142-1123\(01\)00166-9](https://doi.org/10.1016/S0142-1123(01)00166-9) (2001).
15. Jong-Cheon, K., Cheong, S.-K. & Noguchi, H. Evolution of residual stress redistribution associated with localized surface microcracking in shot-peened medium-carbon steel during fatigue test. *Int. J. Fatigue* **55**, 147–157. <https://doi.org/10.1016/j.ijfatigue.2013.06.010> (2013).
16. Zabeen, S., Preuss, M. & Withers, P. J. Residual stresses caused by head-on and 45° foreign object damage for a laser shock peened Ti-6Al-4V alloy aerofoil. *Mater. Sci. Eng.* **560**, 518–527. <https://doi.org/10.1016/j.msea.2012.09.097> (2013).
17. Ren, X., Chen, B., Jiafei Jiao, Yu., Yang, W. Z. & Tong, Z. Fatigue behavior of double-sided laser shock peened Ti-6Al-4V thin blade subjected to foreign object damage. *Opt. Laser Technol.* **121**, 105784. <https://doi.org/10.1016/j.optlastec.2019.105784> (2020).
18. Neuber H. Theory of Notch Stresses: Principles of Exact Calculation of Strength with Reference to Structural Form and Material. US: Clearinghouse for Federal Scientific and Technical Information (1961).
19. Peterson, R. E. The role of stress distribution in fatigue. *Exp. Mech.* **1**(4), 105–115. <https://doi.org/10.1007/bf02323115> (1961).
20. Ruschau, J., Thompson, S. R. & Nicholas, T. High cycle fatigue limit stresses for airfoils subjected to foreign object damage. *Int. J. Fatigue* **25**(9), 955–962. [https://doi.org/10.1016/S0142-1123\(03\)00135-X](https://doi.org/10.1016/S0142-1123(03)00135-X) (2003).
21. Weibull, W. Stockholm, Sweden, a statistical distribution function of wide applicability. *J. Appl. Mechan.* **18**, 293–297 (1951).
22. Zhang, H., Hu, D. & He, C. Y. Experimental and analytical modelling on aeroengine blade foreign object damage. *Int. J. Impact Eng.* **183**, 104813.1-104813.18. <https://doi.org/10.1016/j.ijimpeng.2023.104813> (2024).
23. Zhang, H. et al. A simplified Johnson-Cook model of TC4T for aeroengine foreign object damage prediction. *Eng. Fract. Mechan.* <https://doi.org/10.1016/j.engfracmech.2022.108523> (2022).
24. Taylor, D. Geometrical effects in fatigue: a unifying theoretical model. *Int. J. Fatigue* **21**, 413–420. [https://doi.org/10.1016/S0142-1123\(99\)00007-9](https://doi.org/10.1016/S0142-1123(99)00007-9) (1999).
25. Yoichi, Y., Yusuke, U., Hiroshi, K. Critical distance for fatigue life prediction in aerospace materials. ICAF 2011 Structural Integrity: Influence of Efficiency and Green Imperatives: *Proceedings of the 26th Symposium of the International Committee on Aeronautical Fatigue. Montreal, Canada.* (Springer, 2011). [https://doi.org/10.1007/978-94-007-1664-3\\_25](https://doi.org/10.1007/978-94-007-1664-3_25)
26. Benedetti, M., Fontanari, V. & Bandini, M. A simplified and fast method to predict plain and notch fatigue of shot peened high-strength aluminium alloys under reverse bending. *Surface Coatings Technol.* **243**, 2–9. <https://doi.org/10.1016/j.surfcoat.2011.12.008> (2014).
27. Hudak S. J., K. S. Chan, G. G. Chell, Y-D. Lee, R. C. McClung. A damage tolerance approach for predicting the threshold stresses for high cycle fatigue in the presence of supplemental damage. In: L. David, S. et al (eds) TMS Annual Meeting (2002).
28. Nowell, D., Duó, P. & Stewart, I. F. Prediction of fatigue performance in gas turbine blades after foreign object damage. *Int. J. Fatigue* **25**, 963–969. [https://doi.org/10.1016/S0142-1123\(03\)00160-9](https://doi.org/10.1016/S0142-1123(03)00160-9) (2003).
29. Chaves, V., Madrigal, C. & Navarro, A. Fatigue limit predictions at stress concentrations using FEA and microstructural fracture mechanics. *Theoret. Appl. Fract. Mech.* **87**, 11–20. <https://doi.org/10.1016/j.tafmec.2016.09.011> (2017).
30. Navarro, A. & De Los, R. E. R. An alternative model of the blocking of dislocations at grain boundaries. *Philosophical Mag.* **57**, 37–42. <https://doi.org/10.1080/01418618808204497> (1988).
31. HB5277–1984 Vibration fatigue test method for engine blades and materials. (In Chinese).
32. Junhe, Z. Study on prediction method of high cycle fatigue strength of TC17 titanium alloy blade with foreign object damage. *Nanjing Univ. Aeronaut. Astronaut.* <https://doi.org/10.27239/d.cnki.gnhhu.2020.000056> (2020).
33. Wang, L. et al. Fatigue strength improvement in Ti-6Al-4V subjected to foreign object damage by combined treatment of laser shock peening and shot peening. *Int. J. Fatigue* **155**, 106581. <https://doi.org/10.1016/j.ijfatigue.2021.106581> (2022).
34. Maxwell, D. C. & Nicholas, T. Rapid method for generation of a Haigh diagram for high cycle fatigue. *Fatigue Fract. Mechan.* **29**, 626–641 (1999).
35. Zhou, L. et al. High cycle fatigue limit prediction of foreign object damaged aerofoil samples by the theory of critical distances. *Vacuum* **203**, 111220 (2022).
36. Yao, W., Xia, K. & Gu, Y. On the fatigue notch factor, K<sub>f</sub>. *Int. J. Fatigue* **17**(4), 245–251 (1995).
37. Stephens, R. I. et al. *Metal Fatigue in Engineering* (John Wiley & Sons, 2000).

## Acknowledgements

This work was supported by the National Major Science and Technology Project of China (Grant Number J2019-IV-0014-0082), Natural Science Basic Research Program of Shaanxi (Program No. 2023-JC-QN-0044, No. 2023-JC-QN-0094 and No. 2024JC-YBQN-0065) and the National Vertical Research Projects (XXXX2023XXXX006).

## Author contributions

Kainan Lu and Yibo Shang wrote the main manuscript text. All authors reviewed the manuscript. Kainan Lu: Methodology, Investigation, Formal analysis, Writing—Original Draft, Visualization. Yibo Shang: Conceptualization, Methodology, Supervision, Writing—Review & Editing. Chen Wang: Investigation, Data Curation. Bin Li: Investigation, Data Curation. Xiaosheng Zhang: Investigation, Data Curation. Lingfeng Wang: Resources, Funding acquisition. Zhenhua Zhao: Resources, Funding acquisition. Liucheng Zhou: Resources, Funding acquisition. Wei Chen: Resources, Funding acquisition.

## Declarations

## Competing interests

The authors declare no competing interests.

## Additional information

**Correspondence** and requests for materials should be addressed to Y.S., Z.Z. or L.Z.

**Reprints and permissions information** is available at [www.nature.com/reprints](http://www.nature.com/reprints).

**Publisher's note** Springer Nature remains neutral with regard to jurisdictional claims in published maps and institutional affiliations.

**Open Access** This article is licensed under a Creative Commons Attribution-NonCommercial-NoDerivatives 4.0 International License, which permits any non-commercial use, sharing, distribution and reproduction in any medium or format, as long as you give appropriate credit to the original author(s) and the source, provide a link to the Creative Commons licence, and indicate if you modified the licensed material. You do not have permission under this licence to share adapted material derived from this article or parts of it. The images or other third party material in this article are included in the article's Creative Commons licence, unless indicated otherwise in a credit line to the material. If material is not included in the article's Creative Commons licence and your intended use is not permitted by statutory regulation or exceeds the permitted use, you will need to obtain permission directly from the copyright holder. To view a copy of this licence, visit <http://creativecommons.org/licenses/by-nc-nd/4.0/>.

© The Author(s) 2025